

Multi-UAV Enabled Integrated Sensing and Wireless Powered Communication: A Robust Multi-Objective Approach

Omid Rezaei, Mohammad Mahdi Naghsh*, *Senior Member, IEEE*, Seyed Mohammad Karbasi, *Senior Member, IEEE*, and Mohammad Mahdi Nayebi, *Senior Member, IEEE*

Abstract—In this paper, we consider an integrated sensing and communication (ISAC) system with wireless power transfer (WPT) where multiple unmanned aerial vehicle (UAV)-based radars serve multiple clusters of energy-limited communication users in addition to their sensing functionality. In this architecture, the radars sense the environment in phase 1 (namely sensing phase) and meanwhile, the communications users (nodes) harvest and store the energy from the radar transmit signals. The stored energy is then used for information transmission from the nodes to UAVs in phase 2, i.e., uplink phase. Performance of the radar systems depends on the transmit signals as well as the receive filters; the energy of the transmit signals also affects the communication network because it serves as the source of uplink powers. Therefore, we cast a multi-objective design problem addressing performance of both radar and communication systems via optimizing UAV trajectories, radar transmit waveforms, radar receive filters, time scheduling and uplink powers. The design problem is further formulated as a robust non-convex optimization problem taking into account the user location uncertainty. Hence, we devise a method based on alternating optimization followed by concepts of fractional programming, S-procedure, and tricky majorization-minimization (MM) technique to tackle it. Numerical examples illustrate the effectiveness of the proposed method for different scenarios.

Index Terms—Integrated sensing and communication (ISAC), multi-objective optimization, robust resource allocation, unmanned aerial vehicle (UAV), waveform design, wireless power transfer (WPT).

I. INTRODUCTION

In recent years, driven by enormous demands of concurrent sensing and communication ability, there is a lot of interest in developing a new paradigm referred to as integrated sensing and communication (ISAC) in both academia and industry [2]. Note that researches related to this topic have also been addressed with different terminologies like joint radar communication (JRC) [3]–[5], joint communication and radar sensing (JCAS) [6]–[8], dual-functional radar communication (DFRC) [9], [10], and radar communication (RadCom) [11], [12].

A limited part of this work is accepted for publication in IEEE International Conference on Acoustics, Speech and Signal Processing (ICASSP), Rhodes Island, Greece, June 2023 [1].

O. Rezaei, S. M. Karbasi, and M. M. Nayebi are with the Department of Electrical Engineering, Sharif University of Technology, Tehran, 11155-4363, Iran. M. M. Naghsh is with the Department of Electrical and Computer Engineering, Isfahan University of Technology, Isfahan, 84156-83111, Iran. *Please address all the correspondence to M. M. Naghsh, Phone: (+98) 31-33912450; Fax: (+98) 31-33912451; Email: mm_naghsh@iut.ac.ir

Thanks to its high mobility and flexibility, unmanned aerial vehicle (UAV) has emerged as a key technology in future ISAC systems [13]. Precisely, it is expected that UAVs will bring better coverage and improved sensing and communication services in modern ISAC systems [14].

There are several works in the literature that have considered the UAV-enabled ISAC [9], [15]–[21]. The authors in [15] have considered a sum-rate maximization problem constrained to sensing requirements for given targets in a single UAV-enabled ISAC model. In contrast with the mentioned work that the UAV must provide the communication services and sensing tasks simultaneously, the authors in [16] considered a periodic sensing and communication strategy for their UAV-enabled ISAC model to separate the practical requirements of sensing and communication over time.

It is possible to realize more effective sensing and communication with multi-UAV cooperation compared to a single UAV with limited sensing coverage and communication capability. The work in [17] proposed the problem of UAV sensing range maximization based on mutual sensing interference and the communication capacity constraints in a cooperative multi-UAV network. In [18], the completion time minimization problem for multi-UAV ISAC systems is studied. By considering a given required localization accuracy for radar sensing, the authors in [9] studied maximization of both sum and minimum communication rates under the Cramer-Rao bound constraint of the target localization in a multi-UAV ISAC system. In [19], authors proposed a framework based on the extended Kalman filter to track the ground users in a multi-UAV ISAC network. Then, a UAV swarm-enabled ISAC model in [20] considered a distributed cooperative framework for multi-target tracking. In [21], the resource allocation problem for a multi-UAV ISAC system is addressed via a method based on reinforcement learning.

The aforementioned works assume that UAVs employ information-bearing signals as the radar probing signals as well; this leads to limitation of radar capabilities due to availability of low sensing energy as well as special characteristics of communication signals. This observation is a motivation for the current work in which sensing is performed in wireless power transfer (WPT) phase. Precisely, the main contributions of this paper can be summarized as follows.

- In this paper, we consider a multi-UAV enabled integrated sensing and wireless powered communication (ISWPC), where sensing is done in the WPT phase of the

communication. Consequently, the radar/WPT waveforms can be designed for sensing purpose with more power leading to radar performance improvement. Precisely, in the first phase of our ISWPC model, multiple UAV-based phase modulated continuous wave (PMCW) radars transmit sensing waveforms and then, targets (e.g., non-authorized UAVs [22], [23]) can be detected by filtering the backscattered signals. The energy of these sensing waveforms can also be harvested by the energy-limited ground users¹. Then, in the wireless information transfer (WIT) phase, the users in each cluster can upload their information signals to their associated UAVs.

- The aim is to jointly maximize the minimum radar signal-to-interference-plus-noise ratio (SINR) and minimum throughput of communication users by designing the transmit radar/WPT waveforms, radar receive filters, time scheduling as well as uplink power of users, and UAV trajectories under and user location uncertainty.
- The cast multi-objective robust design problem is non-convex and hence, hard to solve. Therefore, we first adopt the scalarization technique to rewrite the objective as a specific weighted sum of sensing and communication metrics. Then, we devise a method exploiting the concepts of fractional programming, S-procedure, and tricky majorization-minimization (MM) techniques in order to deal with the problem efficiently. Our simulation results show the effectiveness of the multi-UAV enabled ISWPC.
- In addition to proposing a wireless powered model for the UAV-enabled ISAC, which is our main contribution, the following items are also the other contributions of this work: (i) designing the radar receive filters to maximize the minimum sensing SINR in an ISAC model, and (ii) proposing a multi-objective design problem for a joint sensing-communication metric using scalarization technique in an ISAC model.

The rest of this paper is organized as follows. The signal and system models are explained in Section II. In Section III, a multi-objective problem is formulated, and an optimization framework is proposed for dealing with the design problem associated with the ISWPC model. Section IV presents numerical examples to illustrate the effectiveness of the proposed method. Finally, conclusions are drawn in Section V.

Notation: Bold lowercase (uppercase) letters are used for vectors (matrices). The notations $\Re\{\cdot\}$, $\mathbb{E}[\cdot]$, $|\cdot|$, $\|\cdot\|_2$, $(\cdot)^T$, $(\cdot)^H$, $(\cdot)^*$, and $\text{tr}\{\cdot\}$ indicate the real-part, statistical expectation, absolute value, l_2 -norm of a vector, transpose, Hermitian, complex conjugate, and trace of a matrix, respectively. The symbols $[\mathbf{A}]_{i,j}$ and $[\mathbf{a}]_i$ are used for element-wise representation of the matrix \mathbf{A} and vector \mathbf{a} , respectively. The notation $\nabla f(\cdot)$ indicates the gradient of the function f . We denote $\mathcal{CN}(\boldsymbol{\omega}, \boldsymbol{\Sigma})$ as a circularly symmetric complex Gaussian (CSCG) distribution with mean $\boldsymbol{\omega}$ and covariance $\boldsymbol{\Sigma}$. The set \mathbb{R} represents real numbers and \mathbb{R}^N and \mathbb{C}^N are the set of $N \times 1$ real and complex vectors, respectively. The set of $N \times N$ Hermitian and identity matrices are denoted by $\mathbb{H}^{N \times N}$ and

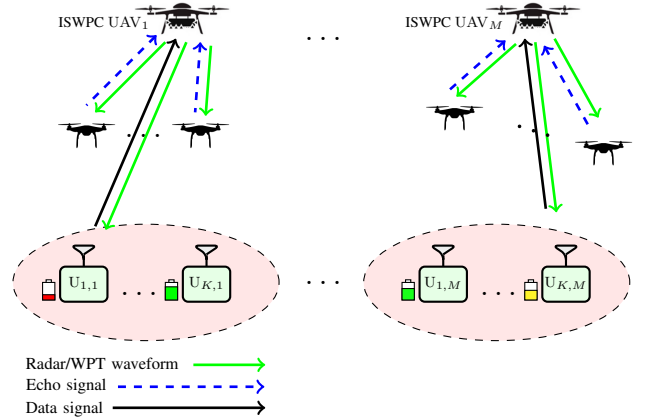


Fig. 1. A multi-UAV enabled ISWPC. The ground users, i.e., $U_{k,m}$, can be considered as traffic/air quality monitoring or fire detector sensors in smart cities, crop/soil monitoring or livestock tracking sensors in farmlands, etc.

\mathbf{I}_N , respectively. The notation $\mathbf{A} \succeq \mathbf{B}$ means that $\mathbf{A} - \mathbf{B}$ is positive semi-definite.

II. SYSTEM MODEL

We consider a multi-UAV enabled ISWPC where M UAVs are employed to serve KM single-antenna ground users denoted by $U_{k,m}$, $1 \leq k \leq K$, $1 \leq m \leq M$, in M clusters and also act as surveillance radars (see Fig. 1). First, the UAVs transmit energy to users and also perform radar sensing. Then, users in each cluster transmit their information signals to their associated UAVs. Each user has an energy harvesting circuit and can store energy for its operation. In this paper, we assume that UAVs are equipped with directional single-antenna with half power beam-width of ζ (in degree) for radar/communication transmitters as well as communication receivers; the radar receivers can have several antennas (i.e., an uniform planar array (UPA) of antennas) to estimate target direction in addition to its range and Doppler. The UAVs are assumed to fly at the time-varying coordinate $\mathbf{q}_m(t) = [x_m(t), y_m(t), z_m(t)]^T \in \mathbb{R}^3$, at time interval $0 \leq t \leq T$. The period T is discretized into N equal time slots where the elemental slot length $\delta_t = T/N$ is chosen to be sufficiently small such that the location of UAVs are considered as approximately unchanged within each time slot δ_t . As a result, the trajectory of m th UAV, denoted by UAV_m , can be approximated by the sequence $\mathbf{q}_m[n] = [x_m[n], y_m[n], z_m[n]]^T$, $1 \leq n \leq N$. The user location information at UAVs, provided e.g., by GPS, may be also imperfect due to radio signal interference [29]. Thus, in this paper, we take into account the user location uncertainty for robust resource allocation. Then, the coordinates of $U_{k,m}$ are modeled as

$$x_{k,m} = \bar{x}_{k,m} + \Delta x_{k,m}, \quad y_{k,m} = \bar{y}_{k,m} + \Delta y_{k,m}, \quad (1)$$

respectively, where $\bar{x}_{k,m}$ and $\bar{y}_{k,m}$ are the user location estimates available at UAVs, and $\Delta x_{k,m}$ as well as $\Delta y_{k,m}$ denote the associated location uncertainties. Furthermore, we assume that UAVs know their own location perfectly [26]–[29]. Then, letting $\mathbf{r}_{k,m} = [x_{k,m}, y_{k,m}]^T$, $\bar{\mathbf{r}}_{k,m} = [\bar{x}_{k,m}, \bar{y}_{k,m}]^T$, and

¹The interested reader may refer to [24]–[28] where ground users harvest energy from UAV signals.

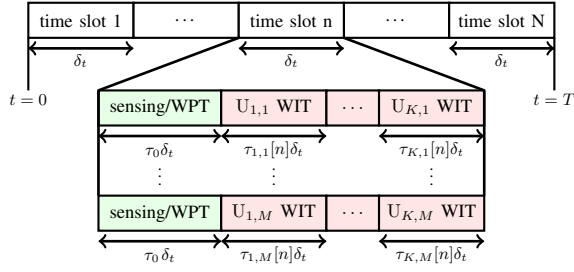


Fig. 2. Protocol structure for multi-UAV enabled ISWPC.

$\Delta \mathbf{r}_{k,m} = [\Delta x_{k,m}, \Delta y_{k,m}]^T$, the distance from UAV_m to U_{k,i} in time slot *n* can be expressed as

$$d_{k,i,m}[n] = \sqrt{\|\tilde{\mathbf{q}}_m[n] - \mathbf{r}_{k,i}\|_2^2 + z_m^2[n]}, \quad (2)$$

where $\tilde{\mathbf{q}}_m[n] = [x_m[n], y_m[n]]^T$. We assume that the communication links from UAVs to the ground users are dominated by the line-of-sight (LoS) links. The channel power gain from UAV_m to U_{k,i} during slot *n* follows the free-space path loss model which can be written as $h_{k,i,m}[n] = \rho_0 d_{k,i,m}^{-2}[n]$, where ρ_0 denotes the channel power at the reference distance $d_0 = 1$ m.

Fig. 2 shows the timing protocol of the proposed method. Each time slot of width δ_t is divided into $K+1$ subslots where the first subslot with duration $\tau_0\delta_t$ is used for sensing/WPT and the other subslots of duration $\tau_{k,m}[n]\delta_t$ are allocated for uplink transmission from users to UAVs.

A. Downlink: Sensing/WPT Phase

The sensing interval consists of L successive transmission of PMCW radar sequences $\tilde{\mathbf{x}}_m \in \mathbb{C}^{\tilde{N}}$, $1 \leq m \leq M$, with total transmission power of $p_m^{dl}[n]$. Note that we consider \tilde{N} as a fixed parameter determined as per radar range resolution and other practical considerations. The l th received signal of a target associated with a given $\tilde{\mathbf{x}}_m$ in UAV_m at the cell under test can be modeled as²

$$\tilde{\mathbf{y}}_{m,l}[n] = \alpha_m[n]\tilde{\mathbf{x}}_m + \sum_{k=-\tilde{N}+1, k \neq 0}^{\tilde{N}-1} \tilde{\alpha}_{m,k}[n] \mathbf{J}_k \tilde{\mathbf{x}}_m + \mathbf{n}_{m,l}[n], \quad \forall n, m, 1 \leq l \leq L, \quad (3)$$

where $\alpha_m[n]$ and $\tilde{\alpha}_{m,k}[n]$ are the complex parameter corresponding to the propagation and backscattering effects from the desired and interfering targets, respectively, $\mathbf{n}_{m,l}[n] \sim \mathcal{CN}(\mathbf{0}, \sigma_{m,l}^2 \mathbf{I}_{\tilde{N}})$ is a noise vector, and \mathbf{J}_k denotes the periodic shift matrix

$$\mathbf{J}_k = \begin{bmatrix} \mathbf{0}_{(\tilde{N}-k) \times k} & \mathbf{I}_{\tilde{N}-k} \\ \mathbf{I}_k & \mathbf{0}_{k \times (\tilde{N}-k)} \end{bmatrix}, \quad k \geq 1, \quad \mathbf{J}_{-k} = \mathbf{J}_k^T. \quad (4)$$

²We do not consider the effect of Doppler shift for intra-pulse code $\tilde{\mathbf{x}}_m$. That is, this effect is incorporated in complex coefficients $\alpha_m[n]$ and $\tilde{\alpha}_{m,k}[n]$ as a constant phase. However, the inter-pulse Doppler shift is non-negligible and will be taken into account in the following. Besides, we ignore the interference from other UAV radars, i.e., UAV_i, $\forall i \neq m$, due to their weak echo signals.

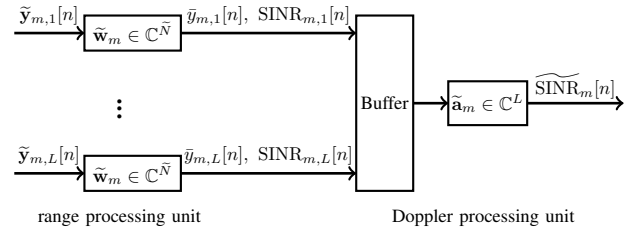


Fig. 3. The block diagram for the radar receiver of the ISWPC UAV_m considering integration over L received signal.

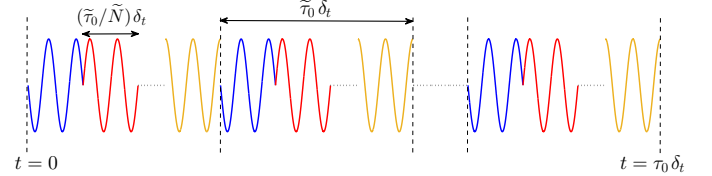


Fig. 4. Illustration of sensing/WPT waveform for the pulse-modulated PMCW radar.

Then, the received signal $\tilde{\mathbf{y}}_{m,l}[n]$ is processed via $\tilde{\mathbf{w}}_m \in \mathbb{C}^{\tilde{N}}$, viz. range processing. The time delay at which each receive filter output signal (i.e., the correlation between $\tilde{\mathbf{w}}_m$ and $\tilde{\mathbf{y}}_m$) has its maximum value can be used to estimate the target range. Following the range processing, Doppler processing is applied on each range-cell to obtain target speed via frequency analysis (usually implemented by FFT) of L samples associated with the range cell (see Fig. 3). Therefore, in practice, it is better to choose L as 2^i , $lb \leq i \leq ub$, where lb and ub are respectively determined according to the minimum required sensing SINR and the allowed system complexity. The sensing/WPT subslot duration can be obtained as $\tau_0\delta_t = L\tilde{\tau}_0\delta_t$ where $\tilde{\tau}_0$ is a fix parameter that can be determined by \tilde{N} and the sampling frequency of radars (see Fig. 4). Using (3), the sensing SINR of UAV_m after range processing block, i.e., the signal $\tilde{\mathbf{y}}_{m,l}[n] = \tilde{\mathbf{w}}_m^H \tilde{\mathbf{y}}_{m,l}[n]$ can be written as

$$\text{SINR}_{m,l}[n] = \frac{|\alpha_m[n]|^2 |\tilde{\mathbf{w}}_m^H \tilde{\mathbf{x}}_m|^2}{\tilde{\mathbf{w}}_m^H \tilde{\mathbf{\Xi}}_{m,l} \tilde{\mathbf{w}}_m}, \quad (5)$$

where

$$\tilde{\mathbf{\Xi}}_{m,l} = \sigma_{m,l}^2 \mathbf{I}_{\tilde{N}} + \sum_{k=-\tilde{N}+1, k \neq 0}^{\tilde{N}-1} \tilde{\sigma}_{m,k}^2 \mathbf{J}_k \tilde{\mathbf{x}}_m \tilde{\mathbf{x}}_m^H \mathbf{J}_k^H, \quad (6)$$

is a positive definite matrix and $\tilde{\sigma}_{m,k}^2 = \mathbb{E}[|\tilde{\alpha}_{m,k}[n]|^2]$. Then, assuming a-priori known target Doppler shift³, the total sensing SINR of UAV_m after Doppler processing block can be obtained as

$$\widetilde{\text{SINR}}_m[n] = \frac{\beta_m |\alpha_m[n]|^2 |\tilde{\mathbf{w}}_m^H \tilde{\mathbf{x}}_m|^2}{\tilde{\mathbf{w}}_m^H \tilde{\mathbf{\Xi}}_m \tilde{\mathbf{w}}_m}, \quad (7)$$

³Several techniques assume a-priori known Doppler frequency (see e.g., [30], [31]); however, in practice, the Doppler shift can be estimated at the receiver, e.g., via a bank of filters matched to different Doppler frequencies [32].

where

$$\beta_m = L + \sum_{i=1}^L \sum_{j=1, j \neq i}^L [\tilde{\mathbf{a}}_m^*]_i [\tilde{\mathbf{a}}_m]_j, \quad (8)$$

with $\tilde{\mathbf{a}}_m \in \mathbb{C}^L$ is the Doppler processing filter⁴, and

$$\tilde{\mathbf{\Xi}}_m = \sum_{l=1}^L \sigma_{m,l}^2 \mathbf{I}_{\tilde{N}} + \beta_m \sum_{k=-\tilde{N}+1, k \neq 0}^{\tilde{N}-1} \tilde{\sigma}_{m,k}^2 \mathbf{J}_k \tilde{\mathbf{x}}_m \tilde{\mathbf{x}}_m^H \mathbf{J}_k^H, \quad (9)$$

is a positive definite matrix. Assuming Swerling I target model, $\alpha_m[n]$ is assumed to be constant over time slots, i.e., $\alpha_m[n] = \alpha_m$, and so $\widetilde{\text{SINR}}_m[n] = \widetilde{\text{SINR}}_m$.

The harvested energy at $U_{k,m}$ for linear energy harvesting model can be expressed as⁵

$$E_{k,m}[n] = \tau_0 \delta_t \epsilon_{k,m} \sum_{i=1}^M h_{k,m,i}[n] p_i^{dl}[n], \quad (10)$$

where $\epsilon_{k,m}$ denotes the energy conversion efficiency. Note that in practice, there is a non-linear characteristic between $E_{k,m}[n]$ and $p_i^{dl}[n]$. However, a linear energy harvesting circuit is considered here to make the ISWPC model more tractable⁶.

B. Uplink: WIT Phase

In the uplink phase, the transmit power of $U_{k,m}$ in time slot n is denoted by $p_{k,m}^{ul}[n]$. The following energy harvesting constraint for $U_{k,m}$ at time slot n should be satisfied:

$$\tau_{k,m}[n] \delta_t p_{k,m}^{ul}[n] \leq \sum_{j=1}^n E_{k,m}[j] + E_{k,m}^0 - \sum_{j=1}^{n-1} \tau_{k,m}[j] \delta_t p_{k,m}^{ul}[j], \quad (11)$$

where $E_{k,m}^0$ is the remaining energy for $U_{k,m}$ from previous time periods⁷. Then, the achievable throughput of $U_{k,m}$ in time slot n is given by⁸

$$R_{k,m}[n] = \tau_{k,m}[n] \delta_t \log_2 \left(1 + \frac{p_{k,m}^{ul}[n] h_{k,m,m}[n]}{\sigma_{c,m}^2} \right), \quad (12)$$

where $\sigma_{c,m}^2$ is the power of the additive white Gaussian noise at the communication receiver of UAV_{*m*}. Thus, the average throughput of $U_{k,m}$ over N time slots is given by $R_{k,m} = \frac{1}{N} \sum_{n=1}^N R_{k,m}[n]$.

⁴For instance, the filter $\tilde{\mathbf{a}}_m$ can be obtained as $\tilde{\mathbf{a}}_m = [1, e^{-j\nu_m}, \dots, e^{-j\nu_m(L-1)}]^T$ as a simple FFT-based Doppler processing filter with ν_m being the normalized Doppler frequency between the UAV_{*m*} and a possible target.

⁵In practice, the minimum required energy for typical energy harvesting circuits can be in the range of $1 \sim 10 \mu\text{W}$ [33].

⁶The interested reader may see [34] for more details about non-linear energy harvesting models.

⁷It is assumed that $E_{k,m}^0$ is associated with sensing-only mode where the system works before employing the proposed protocol in $[0, T]$. Moreover, some parts of $E_{k,m}^0$ can be obtained by solar energy where $U_{k,m}$ has a hybrid solar-RF energy collector circuit [35]. Note that $E_{k,m}^0$ guarantees the reliable energy for uninterrupted communication in the WIT phase.

⁸Notice that UAVs employ coordinated multi-point (CoMP) reception techniques [36], [37] and as a result, the inter-cluster interference is removed.

III. PROBLEM FORMULATION AND THE PROPOSED METHOD

In this section, we cast the optimization problem in which we aim to jointly maximize the minimum radar SINR, i.e., $\min_m \widetilde{\text{SINR}}_m$, and minimum throughput of communication users, i.e., $\min_{k,i} R_{k,i}$, in our ISWPC model by designing the radar/WPT waveforms $\tilde{\mathbf{X}} = \{\tilde{\mathbf{x}}_m, \forall m\}$, radar receive filters $\tilde{\mathbf{W}} = \{\tilde{\mathbf{w}}_m, \forall m\}$, time scheduling parameters $\mathbf{A} = \{\tau_{k,m}[n], \forall k, m, n\}$, integration parameter L , uplink power of users $\mathbf{P}^{ul} = \{p_{k,m}^{ul}[n], \forall k, m, n\}$, and UAV trajectories $\mathbf{Q} = \{\mathbf{q}_m[n], \forall m, n\}$. To find the Pareto-optimal solutions of the mentioned multi-objective problem, we adopt the scalarization technique [38] using the Pareto weight $\mu \in [0, 1]$ as follows

$$\begin{aligned} \max_{\tilde{\mathbf{X}}, \tilde{\mathbf{W}}, \mathbf{A}, L, \mathbf{P}^{ul}, \mathbf{Q}} \quad & (1 - \mu) \min_{\substack{1 \leq k \leq K \\ 1 \leq i \leq M}} \min_{\Delta \mathbf{r}_{k,i}^T, \Delta \mathbf{r}_{k,i} \leq \bar{d}_{k,i}^2} R_{k,i} \\ & + \mu \min_{1 \leq m \leq M} \widetilde{\text{SINR}}_m \end{aligned} \quad (13)$$

s.t.

$$\begin{aligned} \text{C}_1 : & 0 \leq \tau_{k,m}[n] \leq 1 - L\tilde{\tau}_0, \sum_{k=1}^K \tau_{k,m}[n] \leq 1 - L\tilde{\tau}_0, \forall k, m, n, \\ \text{C}_2 : & \|\mathbf{q}_m[n] - \mathbf{q}_m[n-1]\|_2 \leq \delta_t v_{\max}, z_{\min} \leq z_m[n] \leq z_{\max}, \\ & \frac{1}{N} \sum_{n=1}^N z_m[n] \geq z_m^{\text{tr}}, \tilde{\mathbf{q}}_m[n] \in \text{CR}_m, \mathbf{q}_m[0] = \mathbf{q}_m[N], \forall m, n, \\ \text{C}_3 : & \|\tilde{\mathbf{q}}_m[n] - \mathbf{q}_{m,j}^{\text{NFZ}}\|_2 \geq (r_{m,j}^{\text{NFZ}})^2, \forall m, n, 1 \leq j \leq N_m^{\text{NFZ}}, \\ \text{C}_4 : & L \in \{2^{lb}, 2^{lb+1}, \dots, 2^{ub}\}, \text{C}_5 : |\tilde{x}_m(i)|^2 = p_m^{dl}[n], \forall m, i, n, \\ \text{C}_6 : & \sum_{j=1}^n \tau_{k,m}[j] \delta_t p_{k,m}^{ul}[j] \leq \min_{\Delta \mathbf{r}_{k,m}^T, \Delta \mathbf{r}_{k,m} \leq \bar{d}_{k,m}^2} \sum_{j=1}^n E_{k,m}[j] \\ & + E_{k,m}^0, \forall k, m, n, \end{aligned}$$

where $\bar{d}_{k,i}$ denotes the radius of the circular uncertainty region [39], v_{\max} is the maximum speed of the ISWPC UAVs, and CR_m indicates the m th cluster region. Note that the design variables $\tilde{\mathbf{X}}$, L , and \mathbf{Q} are the joint parameters between sensing and communication tasks. The constraint $\frac{1}{N} \sum_{n=1}^N z_m[n] \geq z_m^{\text{tr}}$ in C_2 is considered to bring the desired coverage for a given radar field-of-view (FOV) during the period of T seconds. Precisely, z_m^{tr} can be determined numerically in such a way that the possible targets in CR_m are seen by the UAV_{*m*}. The constraint C_3 introduces the cylindrical no-fly zones (NFZ)s⁹ in each cluster with coordinate center $\mathbf{q}_{m,j}^{\text{NFZ}}$ and radius $r_{m,j}^{\text{NFZ}}$, and C_5 represents the unimodularity constraint of the transmit sequence.

It can be seen that the objective function and constraints $\text{C}_3 - \text{C}_6$ are non-convex and so the problem. Therefore, in the following, we devise a method based on alternating optimization to deal with the non-convex design problem. Tackling subproblems corresponding to aforementioned alternating optimization is associated with novel tricks; e.g., by employing fractional programming, S-procedure, and MM to be discussed shortly.

⁹NFZs are considered due to security, privacy, or safety reasons [40], [41]. Note that the NFZs can also be modeled as a polygonal [42].

A. Maximization over $\widetilde{\mathbf{W}}$ for fixed $[\widetilde{\mathbf{X}}, \mathbf{A}, L, \mathbf{P}^{ul}, \mathbf{Q}]$

We first consider the problem in (13) with respect to (w.r.t.) $\widetilde{\mathbf{W}}$ which is a unconstrained problem. Using the Cauchy-Schwartz inequality, we can write the following expression for SINR_m in the objective function

$$|\widetilde{\mathbf{w}}_m^H \widetilde{\mathbf{x}}_m|^2 = |\widetilde{\mathbf{w}}_m^H \widetilde{\mathbf{\Xi}}_m^{1/2} \widetilde{\mathbf{\Xi}}_m^{-1/2} \widetilde{\mathbf{x}}_m|^2 \leq \left(\widetilde{\mathbf{w}}_m^H \widetilde{\mathbf{\Xi}}_m \widetilde{\mathbf{w}}_m \right) \left(\widetilde{\mathbf{x}}_m^H \widetilde{\mathbf{\Xi}}_m^{-1} \widetilde{\mathbf{x}}_m \right),$$

where the equality holds for

$$\widetilde{\mathbf{w}}_m = \widetilde{\mathbf{\Xi}}_m^{-1} \widetilde{\mathbf{x}}_m, \quad (14)$$

(by neglecting a multiplicative constant) which yields a closed-form solution for $\widetilde{\mathbf{w}}_m$.

B. Maximization over $[\widetilde{\mathbf{X}}, \mathbf{A}, \mathbf{P}^{ul}, \mathbf{Q}]$ for fixed $[\widetilde{\mathbf{W}}, L]$

Then, we consider the problem in (13) w.r.t. $[\widetilde{\mathbf{X}}, \mathbf{A}, \mathbf{P}^{ul}, \mathbf{Q}]$ leading to the associated subproblem. The objective function and the constraints C_3 , C_5 , and C_6 are non-convex. Fig. 5 summarizes the procedure for dealing with this subproblem. First, we aim to deal with the sensing SINR in the objective function which is a non-convex fractional term. We rewrite the second term in the objective function as $f_1(\widetilde{\mathbf{x}}_m) = g_1(\widetilde{\mathbf{x}}_m)/g_2(\widetilde{\mathbf{x}}_m)$ for all m where $g_1(\widetilde{\mathbf{x}}_m) = \widetilde{\mathbf{x}}_m^H \mathbf{\Gamma}_m \widetilde{\mathbf{x}}_m$ and $g_2(\widetilde{\mathbf{x}}_m) = \widetilde{\mathbf{x}}_m^H \widetilde{\mathbf{\Gamma}}_m \widetilde{\mathbf{x}}_m + \gamma_m$ with

$$\mathbf{\Gamma}_m = \mu \beta_m |\alpha_m|^2 \widetilde{\mathbf{w}}_m \widetilde{\mathbf{w}}_m^H, \quad (15)$$

$$\widetilde{\mathbf{\Gamma}}_m = \beta_m \sum_{k=-\widetilde{N}+1, k \neq 0}^{\widetilde{N}-1} \widetilde{\sigma}_{m,k}^2 \mathbf{J}_k^H \widetilde{\mathbf{w}}_m \widetilde{\mathbf{w}}_m^H \mathbf{J}_k, \quad (16)$$

and $\gamma_m = \sum_{l=1}^L \sigma_{m,l}^2 \widetilde{\mathbf{w}}_m^H \widetilde{\mathbf{w}}_m$.

Proposition 1. *Let the objective function of the subproblem in III-B be as follows*

$$q(\widetilde{\mathbf{X}}) = a + \mu \min_{1 \leq m \leq M} f_1(\widetilde{\mathbf{x}}_m), \quad (17)$$

where

$$a = (1 - \mu) \min_{\substack{1 \leq k \leq K \\ 1 \leq i \leq M}} \min_{\Delta \mathbf{r}_{k,i}^T, \Delta \mathbf{r}_{k,i} \leq \widetilde{d}_{k,i}^2} R_{k,i}, \quad (18)$$

is a constant term w.r.t. $\widetilde{\mathbf{X}}$. By exploiting the idea of fractional programming [43] and assuming $g_2(\widetilde{\mathbf{x}}_m) > 0$ (to ensure that $f_1(\widetilde{\mathbf{x}}_m)$ has a finite value), it is proved that the objective function in (17) can be dealt with via iterative maximization of the below function w.r.t. $\widetilde{\mathbf{X}}$:

$$q(\widetilde{\mathbf{X}}) = a + \mu \min_{1 \leq m \leq M} f_2(\widetilde{\mathbf{x}}_m), \quad (19)$$

where

$$f_2(\widetilde{\mathbf{x}}_m) = g_1(\widetilde{\mathbf{x}}_m) - f_1(\widetilde{\mathbf{x}}_m^{(\kappa-1)}) g_2(\widetilde{\mathbf{x}}_m). \quad (20)$$

Proof: Please refer to Appendix A. ■

Then, considering $\|\widetilde{\mathbf{x}}_m\|_2^2 = \widetilde{N} p_m^{dl}[n]$ from the unimodularity constraint C_5 in (13), one can write

$$f_2(\widetilde{\mathbf{x}}_m) = \widetilde{\mathbf{x}}_m^H \mathbf{\Upsilon}_m^{(\kappa-1)} \widetilde{\mathbf{x}}_m, \quad (21)$$

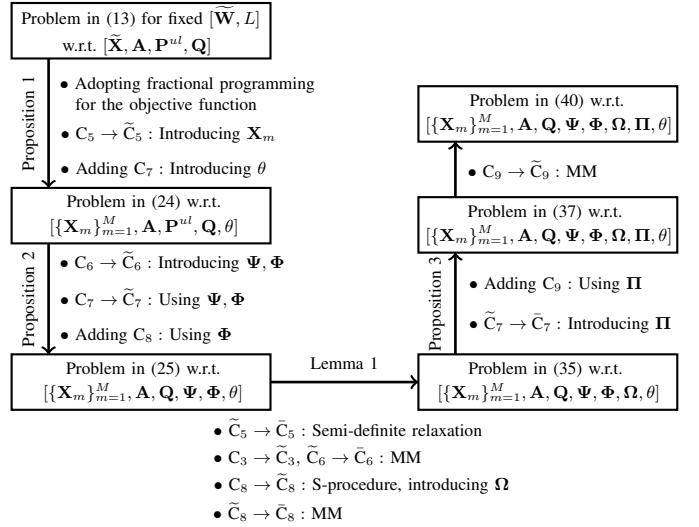


Fig. 5. The diagram of the subproblem in III-B.

where

$$\mathbf{\Upsilon}_m^{(\kappa-1)} = \mathbf{\Gamma}_m - f_1(\widetilde{\mathbf{x}}_m^{(\kappa-1)}) \left(\widetilde{\mathbf{\Gamma}}_m + \frac{\gamma_m}{\widetilde{N} p_m^{dl}[n]} \mathbf{I}_{\widetilde{N}} \right).$$

Now, the second term in the objective function can be written as

$$\min_{1 \leq m \leq M} \widetilde{\mathbf{x}}_m^H \widetilde{\mathbf{\Upsilon}}_m^{(\kappa-1)} \widetilde{\mathbf{x}}_m, \quad (22)$$

where $\widetilde{\mathbf{\Upsilon}}_m = \lambda_m \mathbf{I}_{\widetilde{N}} + \mathbf{\Upsilon}_m$ and λ_m must be selected in such a way that $\widetilde{\mathbf{\Upsilon}}_m$ be a positive definite matrix [44]. Next, by defining a rank-1 matrix $\mathbf{X}_m = \widetilde{\mathbf{x}}_m \widetilde{\mathbf{x}}_m^H$, the quadratic term in (22) can be written as a linear term $\text{tr}(\widetilde{\mathbf{\Upsilon}}_m^{(\kappa-1)} \mathbf{X}_m)$ w.r.t. \mathbf{X}_m , and the constraint C_5 can be expressed as follows

$$\widetilde{C}_5 : [\mathbf{X}_m]_{i,i} = p_m^{dl}[n], \text{rank}(\mathbf{X}_m) = 1, \mathbf{X}_m \succeq \mathbf{0}, \forall m, n, i. \quad (23)$$

By using (23) and the linearized version of (22) as well as introducing an auxiliary variable θ , the problem in (13) for fixed $[\widetilde{\mathbf{W}}, L]$ can be reformulated as

$$\max_{\{\mathbf{X}_m\}_{m=1}^M, \mathbf{A}, \mathbf{P}^{ul}, \mathbf{Q}, \theta} \theta \quad (24)$$

s.t. $C_1 - C_3, \widetilde{C}_5, C_6$,

$$C_7 : (1 - \mu) \min_{\Delta \mathbf{r}_{k,i}^T, \Delta \mathbf{r}_{k,i} \leq \widetilde{d}_{k,i}^2} R_{k,i} + \text{tr} \left(\widetilde{\mathbf{\Upsilon}}_m^{(\kappa-1)} \mathbf{X}_m \right) \geq \theta, \forall k, i, m.$$

Now, to proceed further, we focus on the first term in constraint C_7 and the right-hand side of the constraint C_6 which are associated with the circular uncertainty regions. By introducing $\phi_{k,m,i}[n]$ and applying a change of variable $\psi_{k,m}[n] = \tau_{k,m}[n] p_{k,m}^{ul}[n]$, $\psi_{k,m}[n] \geq 0$, the problem in (24)

can be recast as

$$\begin{aligned}
& \max_{\{\mathbf{X}_m\}_{m=1}^M, \mathbf{A}, \mathbf{Q}, \Psi, \Phi, \theta} \quad \theta \\
& \text{s.t. } \mathbf{C}_1 - \mathbf{C}_3, \tilde{\mathbf{C}}_5, \\
& \tilde{\mathbf{C}}_6 : \sum_{j=1}^n \delta_t \psi_{k,m}[j] \leq \tau_0 \delta_t \epsilon_{k,m} \rho_0 \sum_{j=1}^n \sum_{i=1}^M \frac{p_i^{dl}[j]}{\phi_{k,m,i}[j]} \\
& \quad + E_{k,m}^0, \quad \forall k, m, n, \\
& \tilde{\mathbf{C}}_7 : (1 - \mu) \frac{\delta_t}{N} \sum_{n=1}^N \tau_k[n] \log_2 \left(1 + \frac{\rho_0 \psi_{k,i}[n]}{\sigma_{c,i}^2 \tau_k[n] \phi_{k,i,i}[n]} \right) \\
& \quad + \text{tr} \left(\tilde{\mathbf{Y}}_m^{(\kappa-1)} \mathbf{X}_m \right) \geq \theta, \quad \psi_{k,i}[n] \geq 0, \quad \forall k, i, m, \\
& \mathbf{C}_8 : \|\tilde{\mathbf{q}}_i[n] - (\bar{\mathbf{r}}_{k,m} + \Delta \mathbf{r}_{k,m})\|_2^2 + z_m^2[n] \leq \phi_{k,m,i}[n], \\
& \quad \Delta \mathbf{r}_{k,m}^T \Delta \mathbf{r}_{k,m} \leq \bar{d}_{k,m}^2, \quad \forall k, m, i, n,
\end{aligned} \tag{25}$$

where

$$\Psi = \{\psi_{k,m}[n], \forall k, m, n\}, \tag{26}$$

and

$$\Phi = \{\phi_{k,m,i}[n], \forall k, m, i, n\}. \tag{27}$$

Proposition 2. *The optimal solution of the problem in (24) can be obtained from the solution to the problem in (25).*

Proof: Please refer to Appendix B. \blacksquare

It can be seen that the constraints \mathbf{C}_3 and $\tilde{\mathbf{C}}_5$ - $\tilde{\mathbf{C}}_7$ are still non-convex and \mathbf{C}_8 has an infinite number of constraints due to the continuity of the corresponding user location uncertainty sets. The non-convexity of $\tilde{\mathbf{C}}_5$ originates from the rank-1 constraint. By adopting the semi-definite relaxation, we can drop the rank-1 constraint and proceed to solve the problem.

To proceed further, we can deal with the non-convexity of \mathbf{C}_3 and $\tilde{\mathbf{C}}_6$ in the following. The left-hand side of \mathbf{C}_3 and the first term in the right-hand side of $\tilde{\mathbf{C}}_6$ can be minorized using their supporting hyperplane (see [34] for more details). Therefore, the left-hand side of \mathbf{C}_3 as well as the first term in the right-hand side of $\tilde{\mathbf{C}}_6$ can be respectively obtained at the κ th iteration of the following expressions

$$\begin{aligned}
& \|\tilde{\mathbf{q}}_m^{(\kappa-1)}[n] - \mathbf{q}_{m,j}^{\text{NFZ}}\|_2^2 + 2 \left(\tilde{\mathbf{q}}_m^{(\kappa-1)}[n] - \mathbf{q}_{m,j}^{\text{NFZ}} \right)^T \\
& \quad \times \left(\tilde{\mathbf{q}}_m[n] - \tilde{\mathbf{q}}_m^{(\kappa-1)}[n] \right), \tag{28}
\end{aligned}$$

$$\begin{aligned}
& \tau_0 \delta_t \epsilon_{k,m} \rho_0 \sum_{j=1}^n \sum_{i=1}^M \left\{ \frac{p_i^{dl}[j]}{\phi_{k,m,i}^{(\kappa-1)}[j]} \right. \\
& \quad \left. - \frac{p_i^{dl}[j] \left(\phi_{k,m,i}[j] - \phi_{k,m,i}^{(\kappa-1)}[j] \right)}{\left(\phi_{k,m,i}^{(\kappa-1)}[j] \right)^2} \right\}. \tag{29}
\end{aligned}$$

Next, we consider the constraint \mathbf{C}_8 . Let us introduce a lemma which can be used to transform \mathbf{C}_8 into a finite number of linear matrix inequalities (LMIs).

Lemma 1 (S-procedure). *Let a function $h_m(\mathbf{x}), m \in \{1, 2\}, \mathbf{x} \in \mathbb{C}^N$, be defined as*

$$h_m(\mathbf{x}) = \mathbf{x}^H \mathbf{B}_m \mathbf{x} + 2\Re\{\mathbf{b}_m^H \mathbf{x}\} + b_m, \tag{30}$$

where, $\mathbf{B}_m \in \mathbb{H}^{N \times N}, \mathbf{b}_m \in \mathbb{C}^N$ and $b_m \in \mathbb{R}$. Then, the implication $h_1(\mathbf{x}) \leq 0 \Rightarrow h_2(\mathbf{x}) \leq 0$ holds if and only if there exists an $\omega \geq 0$ such that

$$\omega \begin{bmatrix} \mathbf{B}_1 & \mathbf{b}_1 \\ \mathbf{b}_1^H & b_1 \end{bmatrix} - \begin{bmatrix} \mathbf{B}_2 & \mathbf{b}_2 \\ \mathbf{b}_2^H & b_2 \end{bmatrix} \succeq \mathbf{0}, \tag{31}$$

provided that there exists a point $\hat{\mathbf{x}}$ such that $h_m(\hat{\mathbf{x}}) < 0$.

Proof: Please see [45]. \blacksquare

Then, we can rewrite constraint \mathbf{C}_8 as

$$\begin{aligned}
\mathbf{C}_8 : & \Delta \mathbf{r}_{k,m}^T \Delta \mathbf{r}_{k,m} + 2\Re\{(\bar{\mathbf{r}}_{k,m} - \tilde{\mathbf{q}}_i[n])^T \Delta \mathbf{r}_{k,m}\} \\
& + (\tilde{\mathbf{q}}_i[n] - \bar{\mathbf{r}}_{k,m})^T (\tilde{\mathbf{q}}_i[n] - \bar{\mathbf{r}}_{k,m}) + z_m^2[n] - \phi_{k,m,i}[n] \leq 0.
\end{aligned}$$

Then, using Lemma 1 and considering user location uncertainty region $\Delta \mathbf{r}_{k,m}^T \Delta \mathbf{r}_{k,m} \leq \bar{d}_{k,m}^2$, we can equivalently rewrite the constraint \mathbf{C}_8 as:

$$\begin{aligned}
\tilde{\mathbf{C}}_8 : & \mathbf{S}(\mathbf{Q}, \Phi, \omega_{k,m,i}[n]) = \\
& \begin{bmatrix} (\omega_{k,m,i}[n] - 1) \mathbf{I}_2 & \tilde{\mathbf{q}}_i[n] - \bar{\mathbf{r}}_{k,m} \\ (\tilde{\mathbf{q}}_i[n] - \bar{\mathbf{r}}_{k,m})^T & -\omega_{k,m,i}[n] \bar{d}_{k,m}^2 + \phi_{k,m,i}[n] \\ & -\|\tilde{\mathbf{q}}_i[n] - \bar{\mathbf{r}}_{k,m}\|_2^2 - z_m^2[n] \end{bmatrix} \succeq \mathbf{0}, \tag{32}
\end{aligned}$$

with the variable $\omega_{k,m,i}[n] \geq 0$. Note that the constraint $\tilde{\mathbf{C}}_8$ is still non-convex due to the quadratic term $\|\tilde{\mathbf{q}}_i[n] - \bar{\mathbf{r}}_{k,m}\|_2^2$. For handling this, in light of MM, we construct a global underestimator for the mentioned quadratic term to minorize it and rewrite the constraint $\tilde{\mathbf{C}}_8$ at the κ th iteration as

$$\begin{aligned}
\bar{\mathbf{C}}_8 : & \mathbf{S}(\mathbf{Q}, \Phi, \omega_{k,m,i}[n]) = \\
& \begin{bmatrix} (\omega_{k,m,i}[n] - 1) \mathbf{I}_2 & \tilde{\mathbf{q}}_i[n] - \bar{\mathbf{r}}_{k,m} \\ (\tilde{\mathbf{q}}_i[n] - \bar{\mathbf{r}}_{k,m})^T & -\omega_{k,m,i}[n] \bar{d}_{k,m}^2 + \phi_{k,m,i}[n] \\ & -\chi_{k,m,i}^{(\kappa)}[n] - z_m^2[n] \end{bmatrix} \succeq \mathbf{0}, \tag{33}
\end{aligned}$$

where

$$\begin{aligned}
\chi_{k,m,i}^{(\kappa)}[n] & = \|\tilde{\mathbf{q}}_i^{(\kappa-1)}[n] - \bar{\mathbf{r}}_{k,m}\|_2^2 \\
& + 2 \left(\tilde{\mathbf{q}}_i^{(\kappa-1)}[n] - \bar{\mathbf{r}}_{k,m} \right)^T \left(\tilde{\mathbf{q}}_i[n] - \tilde{\mathbf{q}}_i^{(\kappa-1)}[n] \right), \quad \forall k, m, i, n. \tag{34}
\end{aligned}$$

Now, based on the expressions in (28), (29), and (33), the problem in (25) can be restated as the following

$$\begin{aligned}
& \max_{\{\mathbf{X}_m\}_{m=1}^M, \mathbf{A}, \mathbf{Q}, \Psi, \Phi, \Omega, \theta} \quad \theta \\
& \text{s.t. } \mathbf{C}_1, \mathbf{C}_2, \tilde{\mathbf{C}}_7, \tilde{\mathbf{C}}_3 : (28) \geq (r_{m,j}^{\text{NFZ}})^2, \quad \forall m, n, j, \\
& \tilde{\mathbf{C}}_5 : [\mathbf{X}_m]_{i,i} = p_m^{dl}[n], \quad \mathbf{X}_m \succeq \mathbf{0}, \quad \forall m, n, i, \\
& \tilde{\mathbf{C}}_6 : \sum_{j=1}^n \delta_t \psi_{k,m}[j] \leq (29) + E_{k,m}^0, \quad \forall k, m, n, \\
& \bar{\mathbf{C}}_8 : \mathbf{S}(\mathbf{Q}, \Phi, \Omega) \succeq \mathbf{0}, \quad \omega_{k,m,i}[n] \geq 0, \quad \forall k, m, i, n, \tag{35}
\end{aligned}$$

where

$$\Omega = \{\omega_{k,m,i}[n], \forall k, m, i, n\}. \tag{36}$$

The logarithmic function of the first term in left-hand side of $\tilde{\mathbf{C}}_7$ is a non-concave term and so $\tilde{\mathbf{C}}_7$ is non-convex. By

introducing the auxiliary variables $\pi_{k,i}[n]$, the problem in (35) can be equivalently rewritten as

$$\begin{aligned} & \max_{\{\mathbf{X}_m\}_{m=1}^M, \mathbf{A}, \mathbf{Q}, \Psi, \Phi, \Omega, \Pi, \theta} \theta & (37) \\ \text{s.t. } & \mathbf{C}_1, \mathbf{C}_2, \tilde{\mathbf{C}}_3, \bar{\mathbf{C}}_5, \bar{\mathbf{C}}_6, \bar{\mathbf{C}}_8, \\ & \bar{\mathbf{C}}_7 : (1 - \mu) \frac{\delta_t}{N} \sum_{n=1}^N \tau_k[n] \log_2 \left(1 + \frac{\rho_0 \pi_{k,i}[n]}{\sigma_{c,i}^2 \tau_k[n]} \right) \\ & \quad + \text{tr} \left(\tilde{\mathbf{Y}}_m^{(\kappa-1)} \mathbf{X}_m \right) \geq \theta, \psi_{k,i}[n] \geq 0, \forall k, i, m, \\ & \mathbf{C}_9 : \pi_{k,i}[n] \leq \frac{\psi_{k,i}[n]}{\phi_{k,i,i}[n]}, \forall k, i, n, \end{aligned}$$

where

$$\mathbf{\Pi} = \{\pi_{k,i}[n], \forall k, i, n\}. \quad (38)$$

Proposition 3. *The optimal solution of the problem in (35) can be obtained by solving the problem in (37).*

Proof: Please refer to Appendix B. ■

Then, the non-convexity of \mathbf{C}_9 can be dealt with by minorizing its right-hand side using the following minorizer:

$$\begin{aligned} & \frac{\psi_{k,i}^{(\kappa-1)}[n]}{\phi_{k,i,i}^{(\kappa-1)}[n]} + \frac{1}{\phi_{k,i,i}^{(\kappa-1)}[n]} \left(\psi_{k,i}[n] - \psi_{k,i}^{(\kappa-1)}[n] \right) & (39) \\ & - \frac{\psi_{k,i}^{(\kappa-1)}[n]}{\left(\phi_{k,i,i}^{(\kappa-1)}[n] \right)^2} \left(\phi_{k,i,i}[n] - \phi_{k,i,i}^{(\kappa-1)}[n] \right), \end{aligned}$$

and the problem in (37) can be reformulated as

$$\begin{aligned} & \max_{\{\mathbf{X}_m\}_{m=1}^M, \mathbf{A}, \mathbf{Q}, \Psi, \Phi, \Omega, \Pi, \theta} \theta & (40) \\ \text{s.t. } & \mathbf{C}_1, \mathbf{C}_2, \tilde{\mathbf{C}}_3, \bar{\mathbf{C}}_5 - \bar{\mathbf{C}}_8, \tilde{\mathbf{C}}_9 : \pi_{k,i}[n] \leq (39), \forall k, i, n. \end{aligned}$$

Since the logarithmic term in $\bar{\mathbf{C}}_7$ is jointly concave w.r.t. $\tau_k[n]$ and $\pi_{k,i}[n]$, the constraint $\bar{\mathbf{C}}_7$ and therefore, the problem in (40) are convex and can be solved efficiently by e.g., interior point methods. Note that \mathbf{P}^{ul} can be synthesized after convergence of (40) as follows:

$$p_{k,m}^{ul}[n] = \begin{cases} \psi_{k,m}[n], & \tau_{k,m}[n] \neq 0, \\ 0, & \tau_{k,m}[n] = 0. \end{cases} \quad (41)$$

C. Maximization over L for fixed $[\tilde{\mathbf{X}}, \tilde{\mathbf{W}}, \mathbf{A}, \mathbf{P}^{ul}, \mathbf{Q}]$

As a final step, the problem in (13) w.r.t. the scalar L can be solved via one-dimensional search over its finite possible values in \mathbf{C}_4 .

D. Waveform Synthesis, Convergence, and Complexity Analysis

Algorithm 1 summarizes the steps of the proposed method for jointly maximizing the minimum radar SINR and minimum communication throughput in a multi-UAV enabled ISWPC system. The proposed method consists of outer iterations which are denoted by superscript i . At each outer iteration, we have 3 steps associated with the subproblems in III-A, III-B (which is denoted by superscript κ), and III-C. At the

Algorithm 1 The Proposed Method for Joint Maximization of Minimum Radar SINR and Minimum Communication Throughput in a Multi-UAV ISWPC System

Main-0: Initialize $\mathbf{X}^{(i)}$, $L^{(i)}$, and set $i \leftarrow 0$.

repeat

A: Compute $\tilde{\mathbf{w}}_m^{(i)}$, $\forall m$ via the closed-form solution in (14).

B-0: Initialize $\tilde{\mathbf{W}}^{(\kappa)}$, $L^{(\kappa)}$, $\Phi^{(\kappa)}$, $\Psi^{(\kappa)}$, and set $\kappa \leftarrow 0$.

repeat

B-1: Solve the convex problem in (40).

B-2: Update $\kappa \leftarrow \kappa + 1$.

until convergence

B-3: Synthesize \mathbf{P}^{ul} via (41).

C: Solve the problem in (13) w.r.t. the scalar L via one-dimensional search over its finite possible values in \mathbf{C}_4 .

Main-1: Update $i \leftarrow i + 1$.

until convergence

Main-2: Synthesize $\tilde{\mathbf{x}}_m$ from \mathbf{X}_m .

end of the algorithm, we may synthesize the waveform $\tilde{\mathbf{x}}_m$ from matrix \mathbf{X}_m using e.g., the rank-1 approximation methods based on randomization techniques (see [30] for details).

Note that to ensure convergence to a stationary point, the sequence of objective values of the problem in (13) must be ascending in each subproblem. For the subproblems in III-A and III-C, the global maximum is obtained. Also, applying the proposed fractional programming and MM techniques to the design problem in III-B increases the associated objective function and, under mild conditions, provides stationary points of the problem. Therefore, due to boundedness of the objective function in (13), the sequence of objective values in (13) obtained by the proposed method converges.

Next, the computational complexity of the proposed method is considered. For the subproblem in Subsection III-A, the closed-form expression in (14) must be calculated which needs matrix multiplication and inversion leading to the complexity of¹⁰ $\mathcal{O}(\tilde{N}^3)$ for UAV $_m$. At each inner iterations of the subproblem in III-B, the dominant computational burden is associated with the constraints $\bar{\mathbf{C}}_5$ and $\bar{\mathbf{C}}_8$ due to adopting the semi-definite relaxation. Hence, considering the problem in (40), the computational complexity is $\mathcal{O}(\sqrt{n} \log(1/\epsilon)(mn^3 + m^2n^2 + m^3))$ where $\epsilon > 0$ indicates the solution accuracy, $m = M(1 + MK)$ is the number of semi-definite relaxation-based constraints, and $n = \tilde{N}$ is associated with the size of the related positive semi-definite matrix [47, Theorem 3.12]. Finally, the one-dimensional search in Subsection III-C can be performed via the complexity of $\mathcal{O}(M\tilde{N}^2)$ which comes from the objective function calculations.

Remark 1. *Note that the value of $\widetilde{\text{SINR}}_m$ is greater than $R_{k,i}$ in the objective function of (13) for a typical numerical setup (see Section IV). Therefore, to preserve the controlling role of*

¹⁰This can be decreased to $\mathcal{O}(\tilde{N}^{2.373})$ by using the optimized algorithms (see e.g., [46] for details).

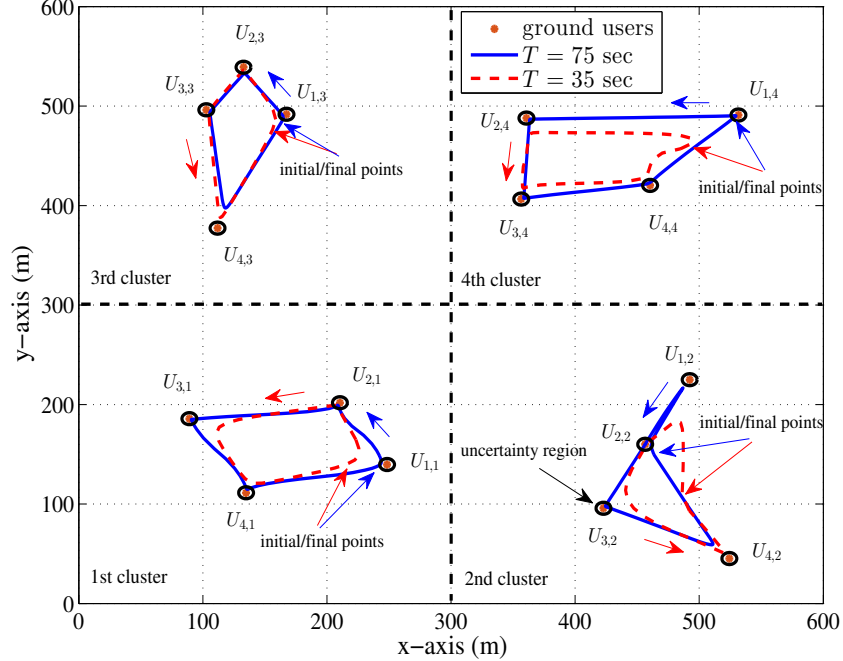


Fig. 6. 2D optimized UAV trajectories for different T .

the Pareto weight μ , we modify the objective function of (13) as follows

$$(1 - \mu) \min_{\substack{1 \leq k \leq K \\ 1 \leq i \leq M}} \min_{\Delta \mathbf{r}_{k,i}^T, \Delta \mathbf{r}_{k,i} \leq d_{k,i}^2} R_{k,i} + \mu \mu_0 \min_{1 \leq m \leq M} \widetilde{\text{SINR}}_m, \quad (42)$$

where $\mu_0 \in (0, 1]$ is a constant parameter which can be determined under the numerical supervision, without losing the optimality of the solution to the problem.

Remark 2. It is worth pointing out that the proposed algorithm can be modified to address the sum throughput/sensing SINR maximization problem. The interested reader may follow the steps in Appendix C for the sum utility problem.

IV. NUMERICAL EXAMPLES

In this section, we evaluate the effectiveness of the proposed method by numerical examples. The convex problem associated with the devised method is solved by CVX [48]. We consider $\widetilde{\text{SIR}}_{m,k} = \frac{|\alpha_m|^2}{\sigma_{m,k}^2} = -10$ dB, $\forall m, k$, and $\widetilde{\text{SNR}}_{m,l} = \frac{|\alpha_m|^2}{\sigma_{m,l}^2} = -10$ dB, $\forall m, l$ for radar receiver; $\tilde{N} = 350$, $\tilde{\tau}_0 = 700$ μ second, $lb = 5$, $ub = 10$, and $p_m^{dl}[n] = 37$ dBm, $\forall m, n$ [24] for radar/WPT waveform; $\sigma_{c,m}^2 = -134$ dBm, $\forall m$ [24] for communication receiver; $\nu_m = 0.05$ radians (for implementing the FFT-based Doppler processing filter), $\forall m$ [25], $\zeta = 30$ degrees, $v_{\max} = 20$ m/s [25], and $\delta_t = 1$ second [49] as UAV flight parameters; $\rho_0 = -30$ dB [25] for channel power gain; $\epsilon_{m,k} = 0.5$, $\forall m, k$ [24], and $E_{m,k}^0 = 1$ mJ, $\forall m, k$ for energy harvesting circuit; and $\text{CR}_m = \{\text{CR}_m^x = 300\text{m} \times \text{CR}_m^y = 300\text{m}\}$, $\forall m$ [49] for cluster regions. Also, we assume $\mu = 0.5$ unless otherwise

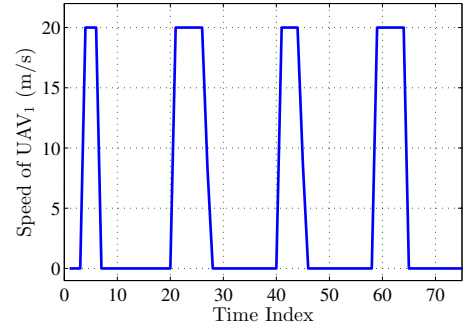


Fig. 7. The speed of UAV₁ for $T = 75$ seconds.

specified. Moreover, we define the normalized radius of user location uncertainty as

$$\tilde{r}_{k,m} = \frac{\tilde{d}_{k,m}}{\min(\text{CR}_m^x, \text{CR}_m^y)}, \quad \forall k, m. \quad (43)$$

A. 2D Flight scenarios

First, we consider a 2D flight setup, i.e., $z_{\max} = z_{\min} = z_m^{\text{tr}} = 100$ m, $\forall m$ [25], with $K = 4$ for ground users which are located in $M = 4$ clusters. Moreover, we set $N_m^{\text{NFZ}} = 0$, $\forall m$, and $\tilde{r}_{k,m} = 0.04$, $\forall k, m$, in this subsection.

Fig. 6 illustrates the optimized UAV trajectories for different T . It can be seen that in order to increase the harvested energy during the sensing/WPT phase, the UAVs adjust their trajectory center to be close to the center of users for all cases. By increasing T , the UAVs try to move closer to each user for increasing the communication throughput during the

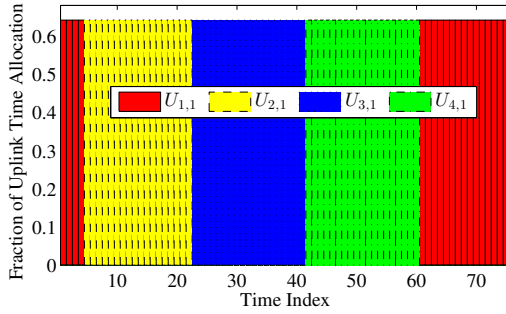


Fig. 8. Optimized time resource allocation of UAV₁ for $T = 75$ seconds.

uplink phase. Precisely, UAVs hover around their cluster users for the maximum possible duration to maintain the closest situation. For instance, the amount of hovering time for UAV₁ can be seen from its speed diagram in Fig. 7 for the case of $T = 75$ seconds, where we can observe that the speed of UAV₁ reduces to zero when flies right above each user.

Moreover, as an example for time scheduling, we illustrate the optimized fraction of the uplink time resource allocation of UAV₁ for the case of $T = 75$ seconds in Fig. 8, where the optimal value of L is equal to 512 and therefore, $\tau_0 = L\tilde{\tau}_0 = 0.3584$ second is obtained for the sensing/WPT phase. We can also observe that in the optimized uplink time scheduling, only one user in each cluster (which is the closest to its associated UAV) is supported at each subslot.

In Fig. 9, the Pareto curves along with the optimized value of L are shown for different values of Pareto weight μ assuming $T = 35$ seconds. It is observed that by increasing μ till 0.85, the minimum sensing SINR is increasing; and minimum communication throughput is decreasing. This is due to the fact that more attention is given to the sensing SINR which is confirmed by looking at larger values for optimal L . For $\mu = 0.85$, L reaches its upper bound 1024 and so, larger μ does not change time scheduling and Pareto curves. Note that since the maximum power budget for uplink transmission are determined by the amount of harvested energy (see (11)), the performance of recharging procedure directly affects the communication throughput. Indeed, the throughput values indicate the performance of both WPT and WIT phases. As a final note, we remark on the fact that the parameter L plays a key role to manage the sensing-communication trade-off.

B. 3D Flight scenarios

In this subsection, we study the general 3D flight mode with $z_{\max} = 150$ m, $z_{\min} = 50$ m, $K = 5$, $M = 2$, $N_1^{\text{NFZ}} = 1$, $N_2^{\text{NFZ}} = 2$, $r_{m,j}^{\text{NFZ}} = 10$ m, $\forall m, j$, $z_m^{\text{tr}} = 85$ m, $\forall m$, and $\tilde{r}_{k,m} = 0.03$, $\forall k, m$.

Fig. 10 shows the UAV trajectories in a 3D scenario. The ability of the proposed method to avoid collision with obstacles in the NFZ can be seen from this figure.

In Fig. 11 we study the effect of user location uncertainty on the communication throughput by comparing the robust and the non-robust schemes. The robust scheme considers the location uncertainties in the resource allocation stage as

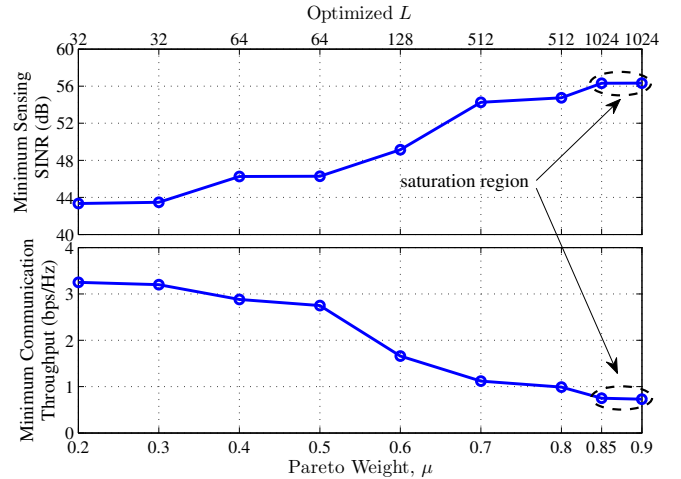


Fig. 9. Pareto-optimized curves for $T = 35$ seconds.

opposed to the non-robust scheme. As expected, by increasing the normalized radius of uncertainty, i.e., $\tilde{r}_{k,m}$, the minimum communication throughput decreases. It can be observed that the performance gain of the robust method over the non-robust one is significant for higher values of $\tilde{r}_{k,m}$.

V. CONCLUSION

In this paper, we proposed a multi-UAV aided ISWPC framework where a dual use of radar/WPT waveforms enables the UAVs to efficiently detect targets and serve a group of energy-limited ground users. We designed the radar receive filters, radar/WPT waveforms, uplink power along with time scheduling of ground users, and UAV trajectories to maximize a joint radar and communication performance metric under user location uncertainty. Through simulations, we demonstrated that ISWPC improves the joint performance of the radar and wireless powered communication, while choosing a suitable value for the total length of radar/WPT sequences. The proposed ISWPC model in this paper can be extended to a class of ISAC optimization problems with other performance metrics under some general constraints, some of which are discussed as follows for future work.

- One can consider the mutual information as the radar performance metric instead of minimum SINR in the cost function of the proposed multi-objective design problem.
- Some practical concepts such as UAV jittering, non-linear energy harvesting circuit, and UPA of antennas for all sensing/communication transmitters and receivers can be taken into account in the design problem.

APPENDIX A PROOF OF PROPOSITION 1

Suppose that $f_2(\tilde{\mathbf{x}}_m) = g_1(\tilde{\mathbf{x}}_m) - f_1(\tilde{\mathbf{x}}_m^{(0)})g_2(\tilde{\mathbf{x}}_m)$, $\forall m$ where $\tilde{\mathbf{x}}_m^{(0)}$ indicates the current value of $\tilde{\mathbf{x}}_m$. Now, let us define $\tilde{\mathbf{x}}_m^* = \arg \max_{\tilde{\mathbf{x}}_m} f_2(\tilde{\mathbf{x}}_m)$, $\forall m$. It is observed that $f_2(\tilde{\mathbf{x}}_m^*) \geq f_2(\tilde{\mathbf{x}}_m^{(0)}) = 0$, $\forall m$. As a result, since $g_2(\tilde{\mathbf{x}}_m) > 0$,

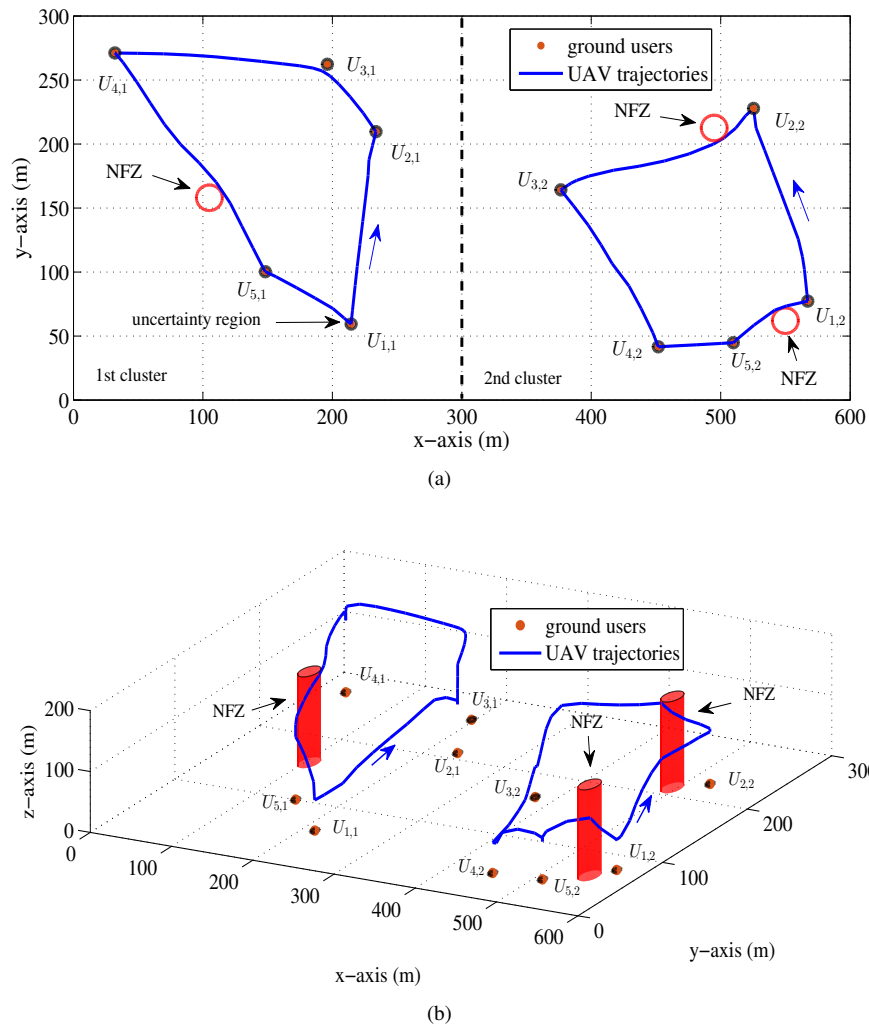


Fig. 10. 3D optimized UAV trajectories for $T = 60$ seconds: (a) bird-view, (b) full-view.

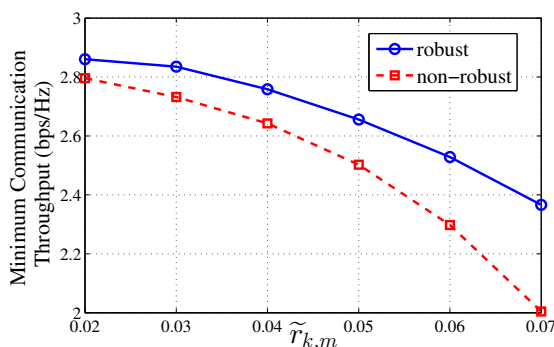


Fig. 11. Minimum communication throughput versus the normalized user location uncertainty for $T = 40$ seconds.

$f_2(\tilde{\mathbf{x}}_m^*) = g_1(\tilde{\mathbf{x}}_m^*) - f_1(\tilde{\mathbf{x}}_m^{(0)})g_2(\tilde{\mathbf{x}}_m^*) \geq 0, \forall m$ leads to $f_1(\tilde{\mathbf{x}}_m^*) \geq f_1(\tilde{\mathbf{x}}_m^{(0)})$, $\forall m$, and therefore, $q(\tilde{\mathbf{X}}^*) \geq q(\tilde{\mathbf{X}}^{(0)})$, where $\tilde{\mathbf{X}}^* = \{\tilde{\mathbf{x}}_m^*, \forall m\}$ and $\tilde{\mathbf{X}}^{(0)} = \{\tilde{\mathbf{x}}_m^{(0)}, \forall m\}$. Consequently, $\tilde{\mathbf{X}}^*$ can be a new matrix $\tilde{\mathbf{X}}$ which increases $q(\tilde{\mathbf{X}})$.

APPENDIX B

PROOF OF PROPOSITION 2 AND PROPOSITION 3

For the case of Proposition 2, we need to prove the following expressions:

- at the optimal solution of the problem in (25), C_8 is active;
- the optimal value of the problem in (24), denoted by θ_{24} , is always greater than the optimal value of the problem in (25), denoted by θ_{25} , and the equality holds when C_8 is active.

Let us proceed by contradiction to prove the first item. To this end, let us assume that at the optimal point of the problem in (25), the equality in C_8 does not hold. In this case, the value of θ can be increased by reducing $\phi_{k,m,i}[n]$ in C_8 , which is evidently in contradiction with the assumption of C_8 is not active.

As to the second item, considering C_7 in (24) and \tilde{C}_8 as well as C_7 in (25), straightforwardly leads to the fact that $\theta_{24} \geq \theta_{25}$ and the equality holds holds when C_8 is active.

The Proposition 3 can be similarly proved.

APPENDIX C
SUM UTILITY MAXIMIZATION PROBLEM

The proposed max-min problem in (13) can be extended to the weighted sum utility maximization problem as follows

$$\begin{aligned} \max_{\tilde{\mathbf{X}}, \tilde{\mathbf{W}}, \mathbf{A}, L, \mathbf{P}^{ul}, \mathbf{Q}} (1 - \mu) \sum_{k=1}^K \sum_{i=1}^M \eta_{k,i}^c \min_{\Delta \mathbf{r}_{k,i}^T, \Delta \mathbf{r}_{k,i} \leq \tilde{d}_{k,i}^2} R_{k,i} \quad (44) \\ + \mu \sum_{m=1}^M \eta_m^s \widetilde{\text{SINR}}_m \end{aligned}$$

$$\text{s.t. } C_1 - C_6,$$

where $\eta_{k,i}^c, \forall k, i$, and $\eta_m^s, \forall m$, denote the communication weights for $U_{k,i}$ and sensing weights for UAV $_m$, respectively. This problem is not convex due to the non-convex objective function and non-convex constraints in $C_3 - C_6$. The maximization procedures over $\tilde{\mathbf{W}}$ and L which are presented in Subsections III-A and III-C can be straightforwardly used here, however, the Subsection III-B must be slightly modified to address the problem in (44). Hence, to deal with the sum of multiple fractional terms in the second term of the objective function in (44), we equivalently recast the problem in (44) for fixed $[\tilde{\mathbf{W}}, L]$ as follows

$$\begin{aligned} \max_{\tilde{\mathbf{X}}, \mathbf{A}, \mathbf{P}^{ul}, \mathbf{Q}, \tilde{\boldsymbol{\theta}}} (1 - \mu) \sum_{k=1}^K \sum_{i=1}^M \eta_{k,i}^c \min_{\Delta \mathbf{r}_{k,i}^T, \Delta \mathbf{r}_{k,i} \leq \tilde{d}_{k,i}^2} R_{k,i} + \mu \sum_{m=1}^M \eta_m^s \tilde{\theta}_m \quad (45) \end{aligned}$$

$$\text{s.t. } C_1 - C_3, C_5, C_6, C_7^{\text{sum}} : \widetilde{\text{SINR}}_m \geq \tilde{\theta}_m, \forall m,$$

where $\tilde{\boldsymbol{\theta}} = \{\tilde{\theta}_m \geq 0, \forall m\}$. It can be seen that the problem in (45) is separable w.r.t. $[\tilde{\mathbf{X}}, \tilde{\boldsymbol{\theta}}]$ and the other design variables i.e., $[\mathbf{A}, \mathbf{P}^{ul}, \mathbf{Q}]$. Firstly, we write the Lagrange function of the problem in (45) w.r.t. $[\tilde{\mathbf{X}}, \tilde{\boldsymbol{\theta}}]$ as

$$\begin{aligned} \mathcal{L}(\tilde{\mathbf{X}}, \tilde{\boldsymbol{\theta}}, \boldsymbol{\varpi}, \boldsymbol{\varsigma}) = (1 - \mu) \sum_{k=1}^K \sum_{i=1}^M \eta_{k,i}^c \min_{\Delta \mathbf{r}_{k,i}^T, \Delta \mathbf{r}_{k,i} \leq \tilde{d}_{k,i}^2} R_{k,i} \quad (46) \\ + \mu \sum_{m=1}^M \eta_m^s \tilde{\theta}_m + \sum_{m=1}^M \varpi_m \left(g_1(\tilde{\mathbf{x}}_m) - \tilde{\theta}_m g_2(\tilde{\mathbf{x}}_m) \right) \\ + \sum_{m=1}^M \sum_{i=1}^{\tilde{N}} \sum_{n=1}^N \varsigma_{m,i,n} \left(|\tilde{x}_m(i)|^2 - p_m^{dl}[n] \right), \end{aligned}$$

where $\boldsymbol{\varpi} = \{\varpi_m, \forall m\}$ and $\boldsymbol{\varsigma} = \{\varsigma_{m,i,n}, \forall m, i, n\}$ are the Lagrange multipliers. Then, using (46), the Karush-Kuhn-Tucker (KKT) conditions [50] for the problem in (45) w.r.t. $[\tilde{\mathbf{X}}, \tilde{\boldsymbol{\theta}}]$ can be written as

$$\frac{\partial \mathcal{L}}{\partial \tilde{\mathbf{X}}} = \sum_{m=1}^M \varpi_m^* \left(\nabla g_1(\tilde{\mathbf{x}}_m^*) - \tilde{\theta}_m^* \nabla g_2(\tilde{\mathbf{x}}_m^*) \right) \quad (47)$$

$$+ \sum_{m=1}^M \sum_{i=1}^{\tilde{N}} \sum_{n=1}^N \varsigma_{m,i,n} \nabla \left(|\tilde{x}_m^*(i)|^2 - p_m^{dl}[n] \right) = 0,$$

$$\frac{\partial \mathcal{L}}{\partial \tilde{\theta}_m} = \mu \eta_m^s - \varpi_m^* g_2(\tilde{\mathbf{x}}_m^*) = 0, \quad \forall m, \quad (48)$$

$$\varpi_m \frac{\partial \mathcal{L}}{\partial \varpi_m} = \varpi_m^* \left(g_1(\tilde{\mathbf{x}}_m^*) - \tilde{\theta}_m^* g_2(\tilde{\mathbf{x}}_m^*) \right) = 0, \quad \forall m, \quad (49)$$

$$C_5, C_7^{\text{sum}}, \varpi_m \geq 0, \quad \forall m, \quad (50)$$

where the superscript * indicates the optimal value of the parameters. Considering the fact that $g_2(\tilde{\mathbf{x}}_m) > 0, \forall m$ for any $\tilde{\mathbf{x}}_m$, the following expressions can be respectively obtained from (48) and (49):

$$\varpi_m^* = \frac{\mu \eta_m^s}{g_2(\tilde{\mathbf{x}}_m^*)}, \quad \tilde{\theta}_m^* = \frac{g_1(\tilde{\mathbf{x}}_m^*)}{g_2(\tilde{\mathbf{x}}_m^*)}, \quad \forall m. \quad (51)$$

Note that considering $\varpi_m = \varpi_m^*$ and $\tilde{\theta}_m = \tilde{\theta}_m^*$, the expressions in (47) and (50) can be obtained from the KKT conditions of the following optimization problem w.r.t. $\tilde{\mathbf{X}}$:

$$\begin{aligned} \max_{\tilde{\mathbf{X}}, \mathbf{A}, \mathbf{P}^{ul}, \mathbf{Q}} (1 - \mu) \sum_{k=1}^K \sum_{i=1}^M \eta_{k,i}^c \min_{\Delta \mathbf{r}_{k,i}^T, \Delta \mathbf{r}_{k,i} \leq \tilde{d}_{k,i}^2} R_{k,i} \quad (52) \\ + \sum_{m=1}^M \varpi_m \left(g_1(\tilde{\mathbf{x}}_m) - \tilde{\theta}_m g_2(\tilde{\mathbf{x}}_m) \right) \end{aligned}$$

$$\text{s.t. } C_1 - C_3, C_5, C_6.$$

Therefore, the optimal solution of (45) can be equivalently obtained from (52) by satisfying the expressions in (51).

Now, we first tackle the problem in (52) for fixed $[\tilde{\boldsymbol{\theta}}, \boldsymbol{\varpi}]$. The proposed techniques in Subsection III-B can be exactly adopted here to handle the non-convex objective function as well as non-convex constraints in C_3, C_5 , and C_6 . After convergence of the subproblem for fixed $[\tilde{\boldsymbol{\theta}}, \boldsymbol{\varpi}]$, the expressions in (51) for $[\tilde{\boldsymbol{\theta}}, \boldsymbol{\varpi}]$ must be checked; if they are not satisfied, a differential update rule must be employed along with restarting the algorithm (for fixed $[\tilde{\boldsymbol{\theta}}, \boldsymbol{\varpi}]$) to ensure holding (51) (see [51] for details).

REFERENCES

- [1] O. Rezaei, M. M. Naghsh, S. M. Karbasi, and M. M. Nayebi, "Resource allocation for UAV-enabled integrated sensing and communication (ISAC) via multi-objective optimization," in *ICASSP 2023 - 2023 IEEE International Conference on Acoustics, Speech and Signal Processing (ICASSP)*, 2023, pp. 1–5.
- [2] A. Hassaniien, M. G. Amin, E. Aboutanios, and B. Himed, "Dual-function radar communication systems: A solution to the spectrum congestion problem," *IEEE Signal Processing Magazine*, vol. 36, no. 5, pp. 115–126, 2019.
- [3] A. Gameiro, D. Castanheira, J. Sanson, and P. P. Monteiro, "Research challenges, trends and applications for future joint radar communications systems," *Wireless Personal Communications*, vol. 100, no. 1, pp. 81–96, 2018.
- [4] Z. Feng, Z. Fang, Z. Wei, X. Chen, Z. Quan, and D. Ji, "Joint radar and communication: A survey," *China Communications*, vol. 17, no. 1, pp. 1–27, 2020.
- [5] T. Zhang, K. Zhu, S. Zheng, D. Niyato, and N. C. Luong, "Trajectory design and power control for joint radar and communication enabled multi-UAV cooperative detection systems," *IEEE Transactions on Communications*, 2022.
- [6] J. A. Zhang, X. Huang, Y. J. Guo, J. Yuan, and R. W. Heath, "Multibeam for joint communication and radar sensing using steerable analog antenna arrays," *IEEE Transactions on Vehicular Technology*, vol. 68, no. 1, pp. 671–685, 2018.
- [7] K. V. Mishra, M. B. Shankar, V. Koivunen, B. Ottersten, and S. A. Vorobyov, "Toward millimeter-wave joint radar communications: A signal processing perspective," *IEEE Signal Processing Magazine*, vol. 36, no. 5, pp. 100–114, 2019.
- [8] S. Hu, X. Yuan, W. Ni, and X. Wang, "Trajectory planning of cellular-connected UAV for communication-assisted radar sensing," *IEEE Transactions on Communications*, vol. 70, no. 9, pp. 6385–6396, 2022.
- [9] X. Wang, Z. Fei, J. A. Zhang, J. Huang, and J. Yuan, "Constrained utility maximization in dual-functional radar-communication multi-UAV networks," *IEEE Transactions on Communications*, vol. 69, no. 4, pp. 2660–2672, 2020.

- [10] R. Liu, M. Li, Q. Liu, and A. L. Swindlehurst, "Dual-functional radar-communication waveform design: A symbol-level precoding approach," *IEEE Journal of Selected Topics in Signal Processing*, vol. 15, no. 6, pp. 1316–1331, 2021.
- [11] F. Zhang, Z. Zhang, W. Yu, and T.-K. Truong, "Joint range and velocity estimation with intrapulse and intersubcarrier Doppler effects for OFDM-based RadCom systems," *IEEE Transactions on Signal Processing*, vol. 68, pp. 662–675, 2020.
- [12] L. G. de Oliveira, B. Nuss, M. B. Alabd, A. Diewald, M. Pauli, and T. Zwick, "Joint radar-communication systems: Modulation schemes and system design," *IEEE Transactions on Microwave Theory and Techniques*, vol. 70, no. 3, pp. 1521–1551, 2021.
- [13] K. Meng, Q. Wu, J. Xu, W. Chen, Z. Feng, R. Schober, and A. L. Swindlehurst, "UAV-enabled integrated sensing and communication: Opportunities and challenges," *IEEE Wireless Communications*, 2023.
- [14] K. Meng, Q. Wu, S. Ma, W. Chen, and T. Q. Quek, "UAV trajectory and beamforming optimization for integrated periodic sensing and communication," *IEEE Wireless Communications Letters*, 2022.
- [15] Z. Lyu, G. Zhu, and J. Xu, "Joint maneuver and beamforming design for UAV-enabled integrated sensing and communication," *IEEE Transactions on Wireless Communications*, vol. 22, no. 4, pp. 2424–2440, 2022.
- [16] K. Meng, Q. Wu, S. Ma, W. Chen, K. Wang, and J. Li, "Throughput maximization for UAV-enabled integrated periodic sensing and communication," *IEEE Transactions on Wireless Communications*, vol. 22, no. 1, pp. 671–687, 2022.
- [17] X. Chen, Z. Feng, Z. Wei, F. Gao, and X. Yuan, "Performance of joint sensing-communication cooperative sensing UAV network," *IEEE Transactions on Vehicular Technology*, vol. 69, no. 12, pp. 15 545–15 556, 2020.
- [18] K. Meng, X. He, Q. Wu, and D. Li, "Multi-UAV collaborative sensing and communication: Joint task allocation and power optimization," *IEEE Transactions on Wireless Communications*, 2022.
- [19] J. Wu, W. Yuan, F. Liu, Y. Cui, X. Meng, and H. Huang, "UAV-based target tracking: Integrating sensing into communication signals," in *2022 IEEE/CIC International Conference on Communications in China (ICCC Workshops)*. IEEE, 2022, pp. 309–313.
- [20] L. Zhou, S. Leng, Q. Wang, and Q. Liu, "Integrated sensing and communication in UAV swarms for cooperative multiple targets tracking," *IEEE Transactions on Mobile Computing*, 2022.
- [21] M. Wang, P. Chen, Z. Cao, and Y. Chen, "Reinforcement learning-based UAVs resource allocation for integrated sensing and communication (ISAC) system," *Electronics*, vol. 11, no. 3, p. 441, 2022.
- [22] A. Guerra, F. Guidi, D. Dardari, and P. M. Djurić, "Networks of UAVs of low complexity for time-critical localization," *IEEE Aerospace and Electronic Systems Magazine*, vol. 37, no. 10, pp. 22–38, 2022.
- [23] I. Guvenc, F. Koohifar, S. Singh, M. L. Sichitiu, and D. Matolak, "Detection, tracking, and interdiction for amateur drones," *IEEE Communications Magazine*, vol. 56, no. 4, pp. 75–81, 2018.
- [24] K. K. Nguyen, A. Masaracchia, V. Sharma, H. V. Poor, and T. Q. Duong, "RIS-assisted UAV communications for IoT with wireless power transfer using deep reinforcement learning," *IEEE Journal of Selected Topics in Signal Processing*, 2022.
- [25] Z. Li, W. Chen, H. Cao, H. Tang, K. Wang, and J. Li, "Joint communication and trajectory design for intelligent reflecting surface empowered UAV SWIPT networks," *IEEE Transactions on Vehicular Technology*, 2022.
- [26] L. Xie, X. Cao, J. Xu, and R. Zhang, "UAV-enabled wireless power transfer: A tutorial overview," *IEEE Transactions on Green Communications and Networking*, vol. 5, no. 4, pp. 2042–2064, 2021.
- [27] L. Xie, J. Xu, and R. Zhang, "Throughput maximization for UAV-enabled wireless powered communication networks," *IEEE Internet of Things Journal*, vol. 6, no. 2, pp. 1690–1703, 2018.
- [28] J. Xu, Y. Zeng, and R. Zhang, "UAV-enabled wireless power transfer: Trajectory design and energy optimization," *IEEE transactions on wireless communications*, vol. 17, no. 8, pp. 5092–5106, 2018.
- [29] M. Cui, G. Zhang, Q. Wu, and D. W. K. Ng, "Robust trajectory and transmit power design for secure UAV communications," *IEEE Transactions on Vehicular Technology*, vol. 67, no. 9, pp. 9042–9046, 2018.
- [30] A. De Maio, Y. Huang, M. Piezzo, S. Zhang, and A. Farina, "Design of optimized radar codes with a peak to average power ratio constraint," *IEEE Transactions on Signal Processing*, vol. 59, no. 6, pp. 2683–2697, 2011.
- [31] M. M. Naghsh, M. Modarres-Hashemi, S. ShahbazPanahi, M. Soltanalian, and P. Stoica, "Unified optimization framework for multi-static radar code design using information-theoretic criteria," *IEEE Transactions on Signal Processing*, vol. 61, no. 21, pp. 5401–5416, 2013.
- [32] P. Stoica, J. Li, and M. Xue, "Transmit codes and receive filters for radar," *IEEE Signal Processing Magazine*, vol. 25, no. 6, pp. 94–109, 2008.
- [33] B. Clerckx, R. Zhang, R. Schober, D. W. K. Ng, D. I. Kim, and H. V. Poor, "Fundamentals of wireless information and power transfer: From RF energy harvester models to signal and system designs," *IEEE Journal on Selected Areas in Communications*, vol. 37, no. 1, pp. 4–33, 2018.
- [34] O. Rezaei, M. M. Naghsh, Z. Rezaei, and R. Zhang, "Throughput optimization for wireless powered interference channels," *IEEE Transactions on Wireless Communications*, vol. 18, no. 5, pp. 2464–2476, 2019.
- [35] H. T. Tran, M. T. Nguyen, G. Ala, F. Viola *et al.*, "Hybrid solar-RF energy harvesting mechanisms for remote sensing devices," *International Journal of Renewable Energy Research (IJRER)*, vol. 12, no. 1, pp. 294–304, 2022.
- [36] L. Xie, J. Xu, and Y. Zeng, "Common throughput maximization for UAV-enabled interference channel with wireless powered communications," *IEEE Transactions on Communications*, vol. 68, no. 5, pp. 3197–3212, 2020.
- [37] L. Liu, S. Zhang, and R. Zhang, "CoMP in the sky: UAV placement and movement optimization for multi-user communications," *IEEE Transactions on Communications*, vol. 67, no. 8, pp. 5645–5658, 2019.
- [38] S. Boyd, S. P. Boyd, and L. Vandenberghe, *Convex optimization*. Cambridge university press, 2004.
- [39] E. Boshkovska, D. W. K. Ng, N. Zlatanov, A. Koelpin, and R. Schober, "Robust resource allocation for MIMO wireless powered communication networks based on a non-linear EH model," *IEEE Transactions on Communications*, vol. 65, no. 5, pp. 1984–1999, 2017.
- [40] K. P. Valavanis and G. J. Vachtsevanos, *Handbook of unmanned aerial vehicles*. Springer, 2015, vol. 1.
- [41] R. Li, Z. Wei, L. Yang, D. W. K. Ng, N. Yang, J. Yuan, and J. An, "Joint trajectory and resource allocation design for UAV communication systems," in *2018 IEEE Globecom Workshops (GC Wkshps)*. IEEE, 2018, pp. 1–6.
- [42] H.-I. Lee, H.-S. Shin, and A. Tsourdos, "UAV collision avoidance considering no-fly-zones," *IFAC-PapersOnLine*, vol. 53, no. 2, pp. 14 748–14 753, 2020.
- [43] W. Dinkelbach, "On nonlinear fractional programming," *Management science*, vol. 13, no. 7, pp. 492–498, 1967.
- [44] M. Soltanalian and P. Stoica, "Designing unimodular codes via quadratic optimization," *IEEE Transactions on Signal Processing*, vol. 62, no. 5, pp. 1221–1234, 2014.
- [45] S. Boyd, S. P. Boyd, and L. Vandenberghe, *Convex optimization*. Cambridge university press, 2004.
- [46] A. M. Davie and A. J. Stothers, "Improved bound for complexity of matrix multiplication," *Proceedings of the Royal Society of Edinburgh Section A: Mathematics*, vol. 143, no. 2, pp. 351–369, 2013.
- [47] I. M. Bomze, V. F. Demyanov, R. Fletcher, T. Terlaky, I. Pólik, and T. Terlaky, "Interior point methods for nonlinear optimization," *Nonlinear Optimization: Lectures given at the CIME Summer School held in Cetraro, Italy, July 1-7, 2007*, pp. 215–276, 2010.
- [48] M. Grant and S. Boyd, "CVX: Matlab software for disciplined convex programming, sept. 2014," Available on-line at <http://cvxr.com/cvx>.
- [49] Z. Wei, F. Liu, D. W. K. Ng, and R. Schober, "Safeguarding UAV networks through integrated sensing, jamming, and communications," in *ICASSP 2022-2022 IEEE International Conference on Acoustics, Speech and Signal Processing (ICASSP)*. IEEE, 2022, pp. 8737–8741.
- [50] H. Benson, "Global optimization algorithm for the nonlinear sum of ratios problem," *Journal of Optimization Theory and Applications*, vol. 112, no. 1, p. 1, 2002.
- [51] H. Vaezy, M. J. Omid, M. M. Naghsh, and H. Yanikomeroglu, "Energy efficient transceiver design in MIMO interference channels: The selfish, unselfish, worst-case, and robust methods," *IEEE Transactions on Communications*, vol. 67, no. 8, pp. 5377–5389, 2019.